PERFORMANCE CHARACTERISTICS OF AN ELECTROMAGNETIC PUMP

by

David Henry Thompson

A Thesis Submitted to the
Graduate Faculty in Partial Fulfillment of
The Requirements for the Degree of
MASTER OF SCIENCE

Major Subject: Nuclear Engineering

Approved:

Iowa State University
Of Science and Technology
Ames, Iowa

1960

TABLE OF CONTENTS

I. INTRODUCTION

Reference designs of several major reactor concepts (1) based on current values of reactor parameters indicate that net plant efficiencies of 300 Mw(e) power reactor plants constructed today would lie between 24% and 31%. Total power costs of these power reactor plants (2) would vary between 9.56 mills per kwhr and 14.72 mills per kwhr. The Eddystone No. 1 Unit of the Philadelphia Electric Company represents the most advanced coal-fired plant under construction in the United States. This super-critical 325 Mw(e) plant is anticipated to operate at a net plant efficiency of 42.6% with total power cost of approximately 6 mills per kwhr.

Power reactor efficiencies comparable to the coal-fired plant efficiency can be achieved at reactor outlet temperatures above 500 C. Liquid metals provide one means of attaining such temperatures without requiring high system pressures. However, until the advent of nuclear power generation, liquid metals technology was primarily limited to the knowledge gained from the use of mercury boilers for power generation and from the use of sodium as an internal combustion engine exhaust valve coolant.

Test loops have been used to obtain much basic information about liquid metals. Corrosion and erosion of container materials, temperature-dependent mass transfer and heat transfer are among the many phenomena that can be investigated with test loops. In addition to the investigation of liquid metals behavior, the reliability and dependability of pumping and fluid metering equipment and other system components may

be determined. Thus, as a means of furthering liquid metals technology, the test loop serves a multiplicity of purposes.

The object of this thesis is to determine the performance characteristics of a small linear induction electromagnetic pump suitable for high temperature liquid metal test loop operation and to investigate methods by which the performance of the pump may be improved.

II. REVIEW OF LITERATURE

The interaction of current and a magnetic field in a liquid conductor was utilized by Northrup (3) in 1907 to produce a hydrostatic pressure of 9 inches of water by using 600 amperes of current in mercury. At that time he postulated that this phenomenon could be utilized as a large capacity ammeter and was likely to result in new and useful applications.

Einstein and Szilard patented in 1928 the idea of an annular induction pump for use with alkali metals. In 1942, Feld and Szilard (4) detailed the calculations necessary to design an annular induction pump for liquid bismuth.

One of the earliest applications of electromagnetic pumping was in the metal casting industry (5). Electromagnetic pumps were used to transfer molten aluminum from furnaces to die casting machinery, eliminating hand ladling or tilting machinery and delivering slag-free metal.

Much descriptive information on electromagnetic pumps is recorded in the literature of the United States and the United Kingdom. However, Watt (6) and Blake (7) were used as the basic reference in electromagnetic pump theory.

Many types of electromagnetic pumps have been developed in the decade since nuclear power gained prominence and they can be classified as follows:

I. Conduction pumps

A. Direct current

B. Alternating current

II. Induction pumps

A. Annular

B. Helical

C. Linear

D. Rotating magnet

All electromagnetic pumps depend upon the interaction between a current and a magnetic field to produce a force on the liquid metal orthogonal to both the direction of current flow and the magnetic field direction. The conduction pumps require high current at low voltage. This current is supplied to the liquid metal in the pump duct through electrodes brazed to the pump duct wall. Rectifiers can be used to supply current to small direct current conduction pumps but the homopolar generator with liquid metal brushes is the only efficient current supply for large pumps. Current requirements of direct current conduction pumps vary from 4,500 amperes at 0.6 volt for a pump (8) capable of pumping 10 gpm of 500 C bismuth at 60 psi head to 250,000 amperes at 2.5 volts for the primary system coolant pump of the EBR II (9) capable of pumping 10,000 gpm of 700 F sodium at 25 psi head.

The low voltage insulation requirement of the direct current conduction pump minimizes the effect of insulation deterioration when operating in highly radioactive areas at high temperature.

Alternating current conduction pumps are basically the same as the direct current conduction pumps. The magnetic circuit must be laminated to reduce eddy current and iron losses. High currents are obtained from

transformers that can be built as an integral part of the pump. Alternating current conduction pump size is limited by power factor considerations and the alternating current conduction pumps are less efficient than direct current conduction pumps.

Alternating current induction pumps depend upon the moving magnetic field of a polyphase winding to induce eddy currents in the liquid metal. The linear induction pump is the most commonly used induction pump and consists of a pump section located between two laminated stators that contain the polyphase windings. Copper side bars connected to the edges of the pump duct serve as a return path for the eddy currents in a manner analogous to the end rings of an induction motor rotor. The linear induction pump operates without a high current power source and the double stator construction facilitates removal of the pump without disturbing the remainder of the system.

One of the largest linear induction pumps constructed is the secondary sodium coolant system pump of the EBR II (10) that has a capacity of 5,000 gpm of 850 F sodium at 40 psi head with a 43% operating efficiency.

Eddy current paths in the liquid metal pumped by an annular induction pump close on themselves, eliminating the need for copper side bars. The annular pump duct is located around a radially laminated central core and inside an outer stator that contains the windings. This construction produces a stronger pump duct than is normal in the linear induction pump but does not allow pump removal without system disturbance.

The helical induction pump closely resembles the induction motor in appearance and operation. The rotating magnetic field of the stator

causes rotation of the liquid metal in the cylindrical duct between the stator and the "blocked" rotor and spiral guide vanes in the duct impart axial motion to the rotating fluid. The helical induction pump is generally used for low flow, high pressure applications.

The rotating magnet induction pump (11) combines features of both the conduction and the induction pump. The pump duct is in the form of a nearly closed circle with welded side bars. A magnet assembly located on both sides of the pump duct and rotated mechanically produces the moving magnetic field. Direct current excitation of the magnet assembly produces high magnetic field strength and the power factor of the pump is the near unity power factor of the motor. The rotational velocity of the pump can be varied and the rotation provides cooling for the magnet assembly.

III. REVIEW OF THEORY

High electromagnetic pump efficiency requires a small air gap, high magnetic field strength, low slip velocity, and low resistivity liquid metal. The limitation imposed on the magnetic field strength by tooth saturation, the requirement of large duct cross section to reduce hydraulic losses, and the need of sufficient slot depth to allow coil cooling at the expense of power factor and useable flux are among the compromises involved in linear induction electromagnetic pump design. These compromises between the electrical and hydraulic requirements result in a low efficiency.

Induction pumps incur losses having no parallel in induction motors. The finite length of the linear stators and the resulting discontinuity of the traveling magnetic field produce a stationary pulsating magnetic field at each end of the induction pump. The transient currents produced in the liquid metal by the pulsating field further reduce pumping efficiency.

The sharing of current between the metallic pump duct wall and the liquid metal is common to all electromagnetic pumps. The average current in the liquid metal, per unit of pump duct length, is

$$I = \frac{s v_s t B_m}{\sqrt{2}\,\rho} \qquad (1)$$

where

s = slip

v_s = velocity of the magnetic field

t = thickness of the pump duct parallel to the magnetic field

B_m = maximum value of the magnetic field

ρ = resistivity of the liquid metal

Slip in the induction pump is calculated in the same manner as for an induction motor.

$$s = \frac{v_s - v}{v_s} \tag{2}$$

where

v = velocity of the liquid metal on the pump duct

The average current in the pump duct wall, per unit of pump duct length, is

$$I_w = \frac{2v_s\, t_w\, B_m}{\sqrt{2}\ \rho_w} \tag{3}$$

where

t_w = thickness of the pump duct wall

ρ_w = resistivity of the pump duct wall material

Equations (1) and (3) are developed for the fully wound central region of a linear induction pump possessing infinite width or finite width with conducting side bars. The side bars offer negligible resistance to eddy current flow parallel to the direction of fluid flow.

The ratio of current in the pump duct wall to current in the liquid metal at any fluid velocity varies inversely with the slip.

$$\frac{I_w}{I} = \frac{2t_w\, \rho}{t\ \rho_w\, s} \tag{4}$$

The wall loss parameter, also known as the wall/liquid conductivity ratio,

X, is defined as

$$X = \frac{2t_w \rho}{t \rho_w} \tag{5}$$

Thus, equation (4) can be expressed as

$$\frac{I_w}{I} = \frac{X}{s} \tag{6}$$

The maximum electrical efficiency of the pump section is governed by the wall loss parameter.

$$\eta_e = \frac{1 - s}{1 + \frac{X}{s}} \tag{7}$$

The theoretical efficiency of the pump section in a fully wound central region of a linear induction pump is

$$\eta_t = \eta_e \eta_h \tag{8}$$

where η_h is the hydraulic efficiency. The calculation of theoretical efficiency does not include the end losses due to the stationary pulsating magnetic field or the eddy currents induced in the liquid metal outside of the magnetic field.

The average pressure developed in the pump duct per unit of length in the central region of a fully wound linear induction pump is

$$p = \frac{\sigma v_s B_m^2}{2 \rho} \tag{9}$$

If equation (9) is valid over the entire length of the pump, the total

developed pressure would be

$$p = \frac{sv_s\, n\lambda\, B_m^2}{2\rho} \tag{10}$$

where

$n\lambda$ = effective length of the pump

or

$$p = \frac{(v_s - v)\, n\lambda\, B_{rms}^2}{\rho} \tag{11}$$

Power loss in the liquid metal results from the I^2R losses of the eddy currents in the liquid metal.

$$P = \frac{(sv_s)^2\, t\, w\, n\lambda\, B_m^2}{2\rho} \tag{12}$$

where

t = thickness of the pump duct parallel to the magnetic field

w = width of the pump duct parallel to current flow

$n\lambda$ = effective length of the pump

Power loss in the pump duct wall results from the I^2R losses of eddy currents in the pump duct wall.

$$P_w = \frac{v_s^2\, t_w\, w\, n\lambda\, B_m^2}{\rho_w} \tag{13}$$

The ideal power output in the liquid metal is

$$P_o = \frac{v_s^2\, t\, w\, n\lambda\, B_m^2\, (1 - s)\, s}{2\rho} \tag{14}$$

The liquid metal power loss, pump duct wall power loss, and the output power are related by wall loss parameter and slip. Comparison of equations (12), (13), and (14) shows that

$$P_w = \frac{X}{(1 - s)\, s} P_o \tag{15}$$

$$P = \frac{s}{1 - s} P_o \tag{16}$$

$$P_w = \frac{X}{s^2} P \tag{17}$$

Power losses in the liquid metal and the pump duct wall do not constitute the total induction pump power loss. However, the other losses are small in comparison.

The actual power output in the liquid metal is determined from

$$(P_o)_{actual} = (p)_{actual}\, t\, w\, v \tag{18}$$

The actual operating efficiency of a linear induction pump is given by

$$\eta = \frac{(P_o)_{actual}}{\text{total input power}} \tag{19}$$

IV. OBJECT OF THE INVESTIGATION

Bismuth and other liquid metals are capable of dissolving sufficient fissionable material to make them attractive as reactor fuels. Unsuitable properties of many container materials require the use of refractory metals to contain these liquid metals at high temperatures. However, at these temperatures the refractory metals must be protected from the atmosphere because of poor oxidation resistance.

Efficiency considerations would dictate the choice of a conduction pump for circulating bismuth and other heavy liquid metals. The requirement of a high current power supply for the conduction pump and attendant problems of double wall pump section design to combat metal oxidation relegate efficiency to a matter of secondary importance. However, the problems presented by the conduction pump have necessitated the use of a linear induction pump for high temperature test loop operation.

The linear induction pump has proven its ability to operate at temperatures near 1000 C for long periods of time (12). It was previously used to insure circulation in test loops without regard to maintenance of a specific flow rate. The only available information on performance of this pump was that it would pump 85 pounds of 400 C bismuth per minute at a 1/2-inch bismuth head (13).

The desirability of constructing test loops in which design conditions of flow rate and heat transfer can be maintained have necessitated the determination of performance characteristics of the linear induction pump.

V. DESCRIPTION OF EQUIPMENT AND PROCEDURES

The linear induction pump shown in Figure 1 is a two pole, three coil, Y connected, three phase pump. The pump consists of an upper and a lower stator with the three coils located in the lower stator. The pole pitch of the pump is six inches and produces a magnetic field velocity of 60 feet per second at 60 cycles per second power frequency. Each stator contains 76 laminations of 24 gauge hot rolled high silicon magnet core iron with dimensions as shown in Figure 2. The laminations are insulated from each other with 0.005-inch mica sheet. The two outer coils of 140 turns and the center coil of 120 turns are wound of 12 gauge heavy formvar insulated copper magnet wire.

Pump sections with duct thicknesses of 0.063, 0.125, 0.187, and 0.250 inch were fabricated from 0.752 inch OD tantalum tubing (0.030-inch wall thickness) sheathed with 3/4-inch (nominal) schedule 40 inconel pipe.

Mercury, a typical heavy metal with high resistivity, high density, and high viscosity, was the liquid metal used in this experiment. The use of mercury circumvented problems involving welded loop construction and the use of radiography to take pressure head measurements that would have been encountered by using another of the heavy metals.

A venturi meter was used to measure mercury flow because of inherently good accuracy and low hydraulic loss of this flow measuring instrument. The venturi meter was constructed to the proportions recommended by the Committee on Flow Measurement of the International Organization for Standardization (14, p. 45). The ideal equation for the venturi

Figure 1. Linear induction pump and pump section

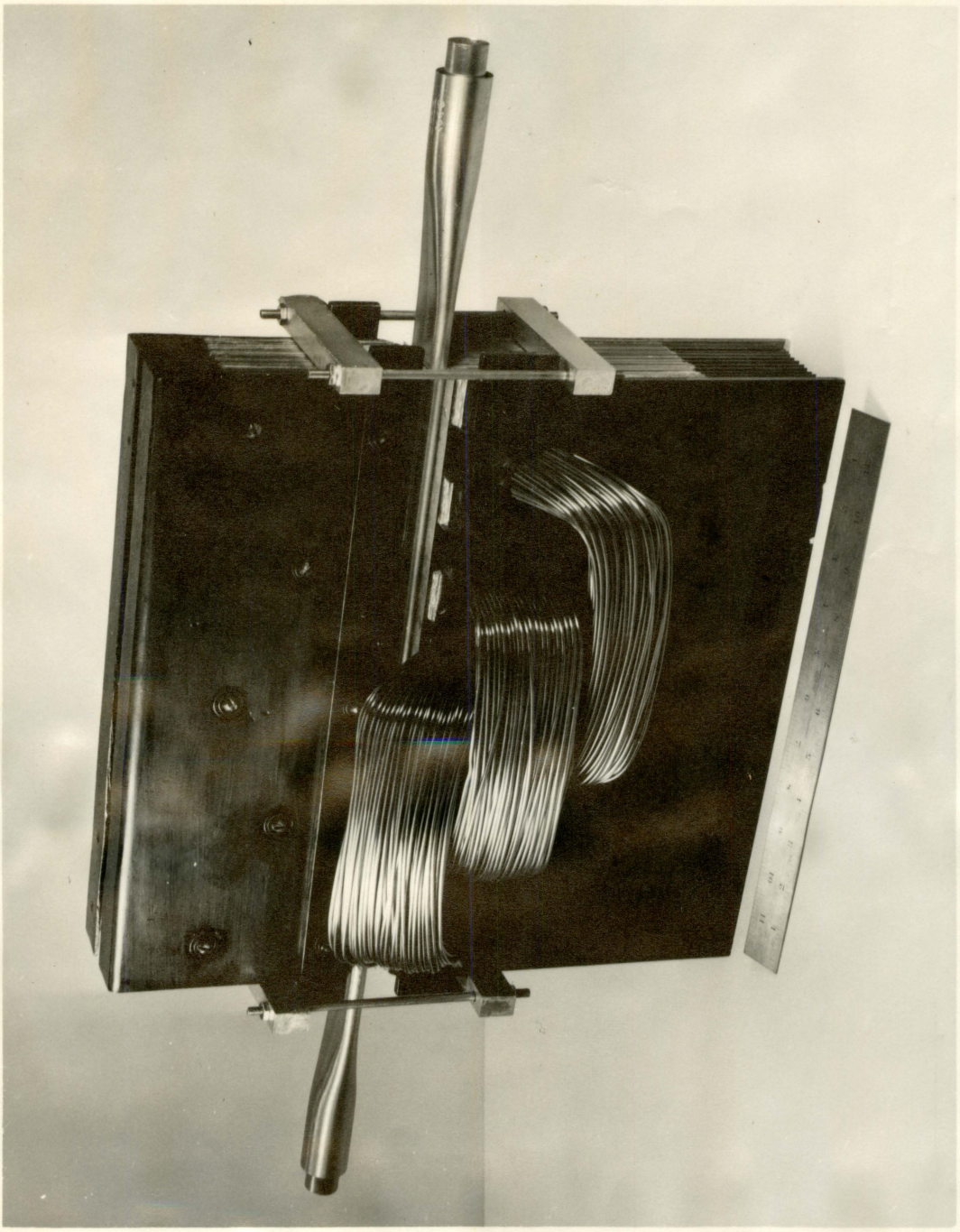

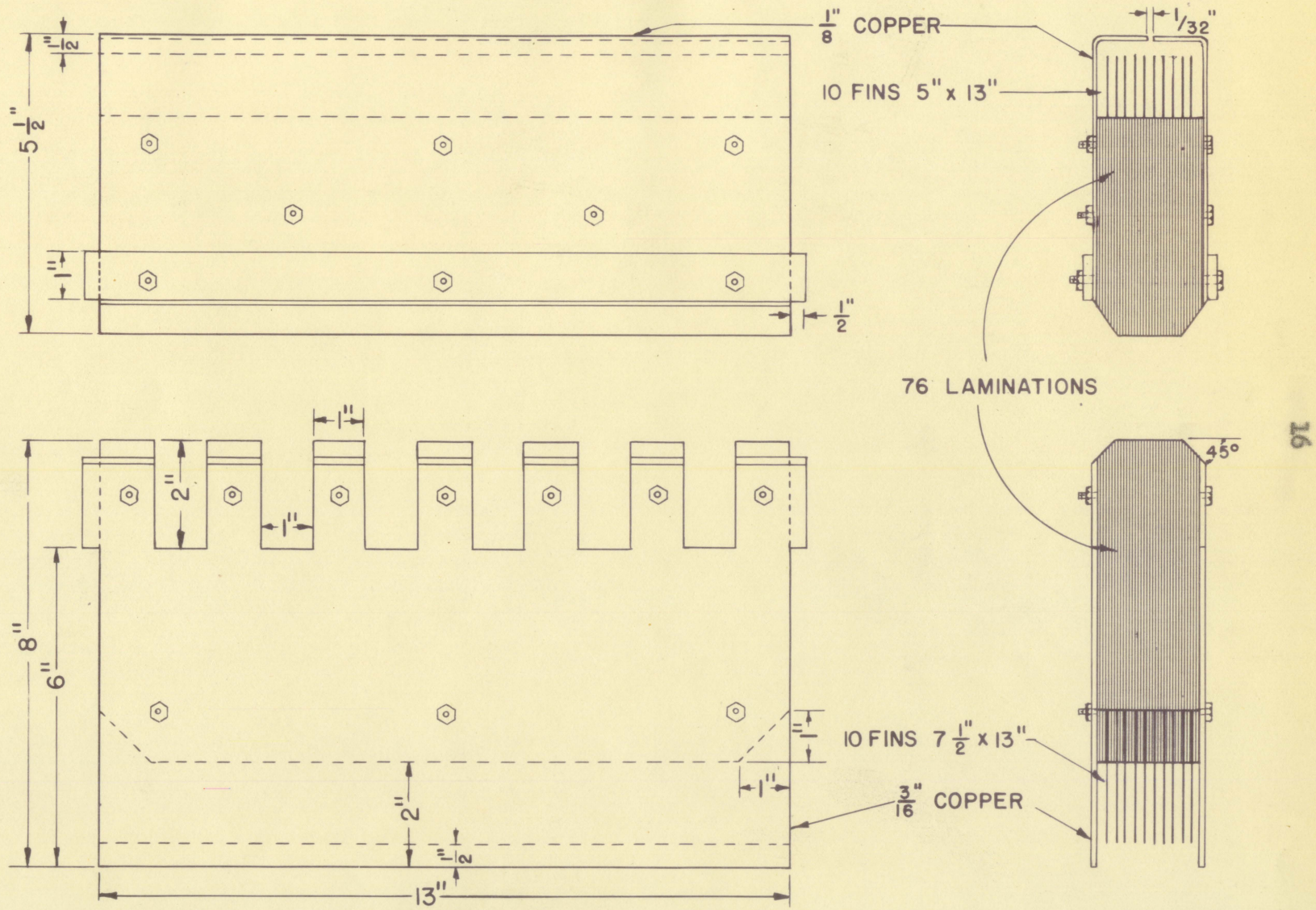

Figure 2. Geometry of linear induction pump stators

meter was developed from the Bernoulli equation and the continuity equation for incompressible fluids. The actual pressure head-flow relationship was determined by using a Viking positive displacement pump to circulate mercury at known flow rates. The discharge coefficients of the venturi meter were determined as the ratio of pressure head at actual flow to that predicted from the ideal equation.

Pump output was controlled by controlling the input voltage with a type 136-3Y three phase Powerstat variable transformer rated at 20 amperes, 240 volts, and 9.7 kva. All three phase readings were taken from a Westinghouse type TA industrial analyzer. Individual phase readings were obtained with a Simpson 269 ultra high sensitivity volt ohm microammeter, a Simpson 15 amp ammeter, and a Weston model 310 single phase wattmeter.

Hydraulic losses in the pump sections were calculated from pressure drop measurements made with water. The equivalence of friction factor in a geometrically similar system at a constant Reynolds number provided the basis for the calculations. The pressure drop relationship between mercury and water for the pump sections tested was obtained from the Darcy equation, as derived in the Appendix.

VI. OUTLINE OF EXPERIMENTS AND RESULTS

A. Basic Performance Characteristics

The performance characteristics of the linear induction pump with a pump section of 0.125-inch duct thickness are shown in Figure 3. The largest measured flow rate of 0.476 gpm through the 0.112 sq in. cross section at a velocity of 1.365 feet per second produced a Reynolds number of 19,740 in the pump duct and a slip of 97.8%. The high Reynolds number and resulting hydraulic losses are indicative of heavy liquid metals and severely limit the flow rate, as indicated in Figure 3.

The wall loss parameter, X, from equation (5), for this pump duct, neglecting the outer inconel sheath of the pump section, is 3.456. Thus, because the pump is operating at near 100% slip, the average current in the tantalum pump duct wall is approximately 3.5 times larger than the average current in the mercury.

The ideal power losses computed from equations (15) and (16) with wall loss parameter X = 3.456 and slip = 0.978 yield $P_w = 160.5\ P_o$ and $P = 44.5\ P_o$. Note the preponderance of loss in the pump duct wall and total power loss of over 200 times the actual output power. Calculation of the ideal efficiency is unnecessary as the magnitudes of power loss suffice to explain the very low efficiency.

The performance characteristics of the pump with a pump section having a 0.250-inch duct thickness are shown on Figure 4. The effect of the reduced magnetic field strength at the increased air gap is evident in the lower pressures developed. Also clearly evident is the much

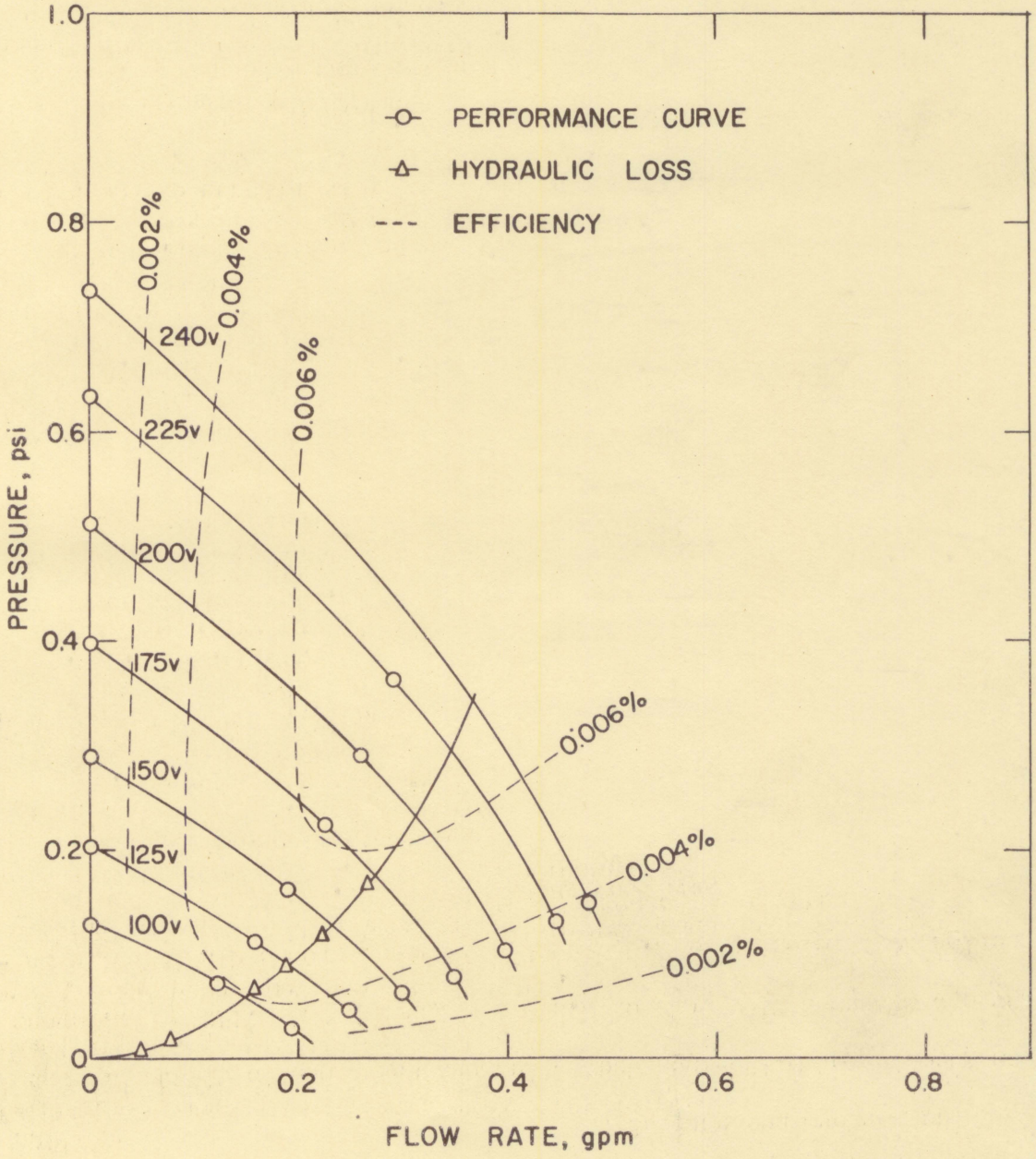

Figure 3. Induction pump performance characteristics (76 laminations, 0.125-inch duct thickness, 0.319-inch air gap).

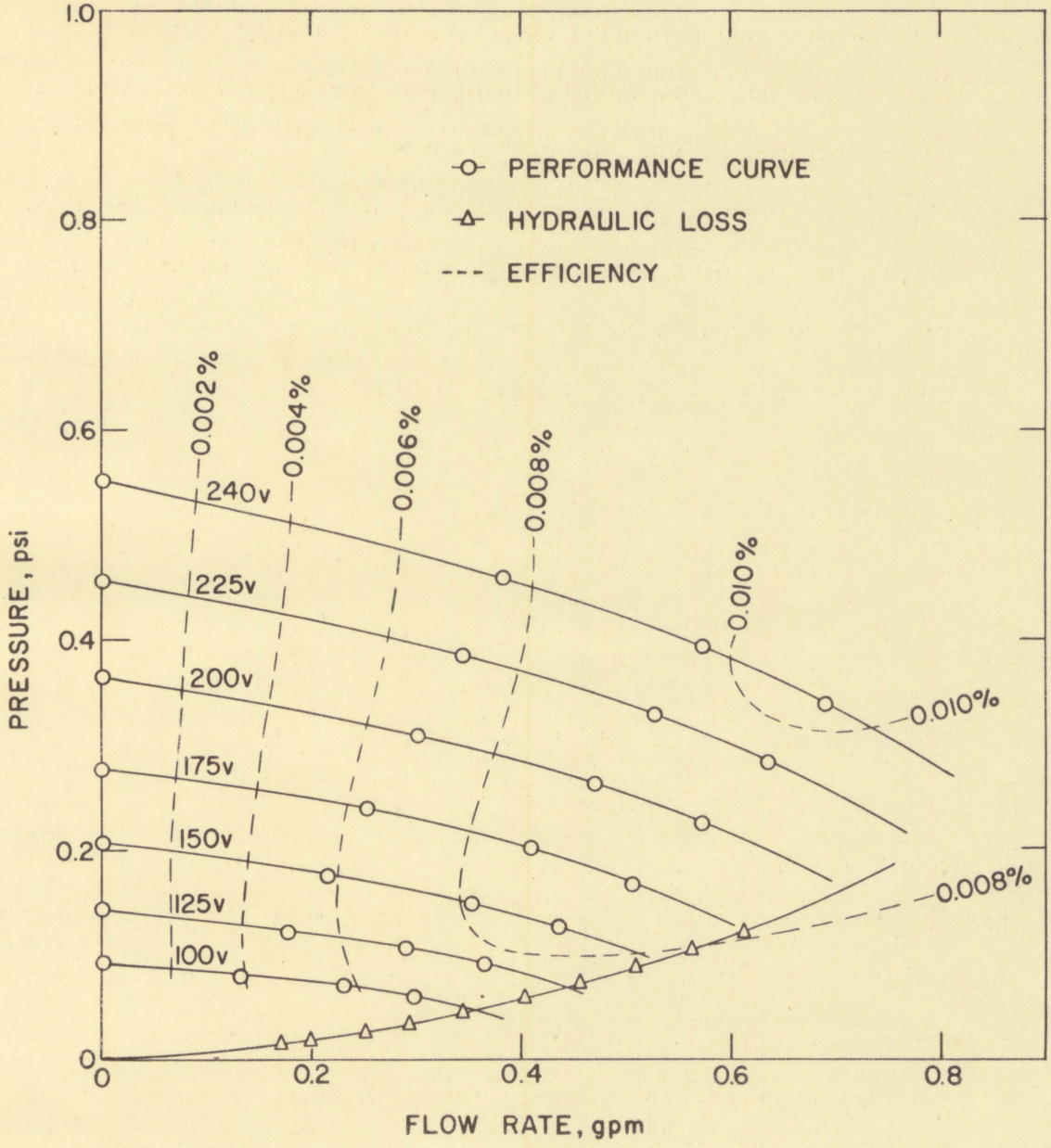

Figure 4. Induction pump performance characteristics (76 laminations, 0.250-inch duct thickness, 0.443-inch air gap)

decreased hydraulic loss resulting from the increase in pump duct cross section from 0.112 sq in. to 0.209 sq in. The flow rate of 0.690 gpm produced a velocity of 1.055 feet per second in the pump duct at a Reynolds number of 29,400 and a slip of 98.2%. The wall loss parameter for this pump duct is 1.656 and at the slip of 0.982, $P_w = 96\ P_o$ and $P = 56\ P_o$. Thus, although the power loss in the mercury is greater than that for the 0.125-inch duct thickness, the wall loss is sufficiently decreased to decrease the total power loss. The total power loss of $162\ P_o$ is 79% of the total power loss in the 0.125-inch duct and the decreased power loss for the larger duct is indicated on Figure 4 as increased efficiency.

Although the over-all operating efficiency of this pump is very low, correspondingly low efficiencies have been noted for an alternating current conduction pump circulating bismuth at similar flow rates (15).

The characteristics of the pump with pump sections of different duct thicknesses will be typical of the characteristics described. Higher pressures can be generated in pump ducts of decreased thickness and decreased over-all pump section air gap at the expense of hydraulic efficiency. The large air gap necessary with pump sections having large duct thicknesses reduces the pressure that can be generated, but improves hydraulic efficiency. This is one example of the compromise necessary between linear induction pump electrical and hydraulic requirements.

B. Stator Modification

The improvement in magnetic field strength and resulting pressure increase with decrease in air gap gave rise to the idea of increasing excitation and magnetic field strength by decreasing the amount of iron in the stators. The pump section with 0.250-inch duct thickness was utilized for comparison purposes. Tabulated in Table 1 are the effects of lamination change at constant voltage.

Table 1. Pump parameters at constant voltage

Laminations	voltage, volts	phase current, amperes	power, watts	no-flow pressure, psi
76	200	15.8	610	0.360
66	200	16.6	690	0.382
56	200	17.1	750	0.430
47	200	18.7	925	0.476

The decreasing impedance of the stators with decrease in number of laminations produces a corresponding increase in average phase current and in power consumed. The increase in no-flow pressure with decrease in number of laminations is directly attributable to the increase in phase current.

Perhaps a better method of illustrating the effect of lamination change would be to use constant phase current as the basis of comparison. In Table 2 are tabulated the pump parameters at constant phase current.

Table 2. Pump parameters at constant phase current

laminations	voltage, volts	phase current, amperes	power, watts	no-flow pressure, psi
76	235	18.7	930	0.515
66	224	18.7	920	0.480
56	217	18.7	915	0.491
47	200	18.7	925	0.476

The nearly constant power consumption and no-flow pressure at the average phase current of 18.7 amperes indicate that the postulated improvement in magnetic field strength at constant current with a decrease in laminations failed to materialize.

The slight improvement of maximum pressure generated by the 47 lamination pump, as shown in Figure 5, over that of the 76 lamination pump (Figure 4) was produced at a current overload condition in the variable autotransformer. This improvement was insufficient to warrant the overload conditions in the autotransformer and pump windings and the added cooling capacity necessary for continuous pump operation.

C. Side Bars

The use of side bars as a means of reducing resistance to eddy current flow has been supported in the literature. It has been found (16) for a pump duct width of four to five times the pole pitch or under conditions of low slip that the side bars can be eliminated without adversely affecting the pump performance.

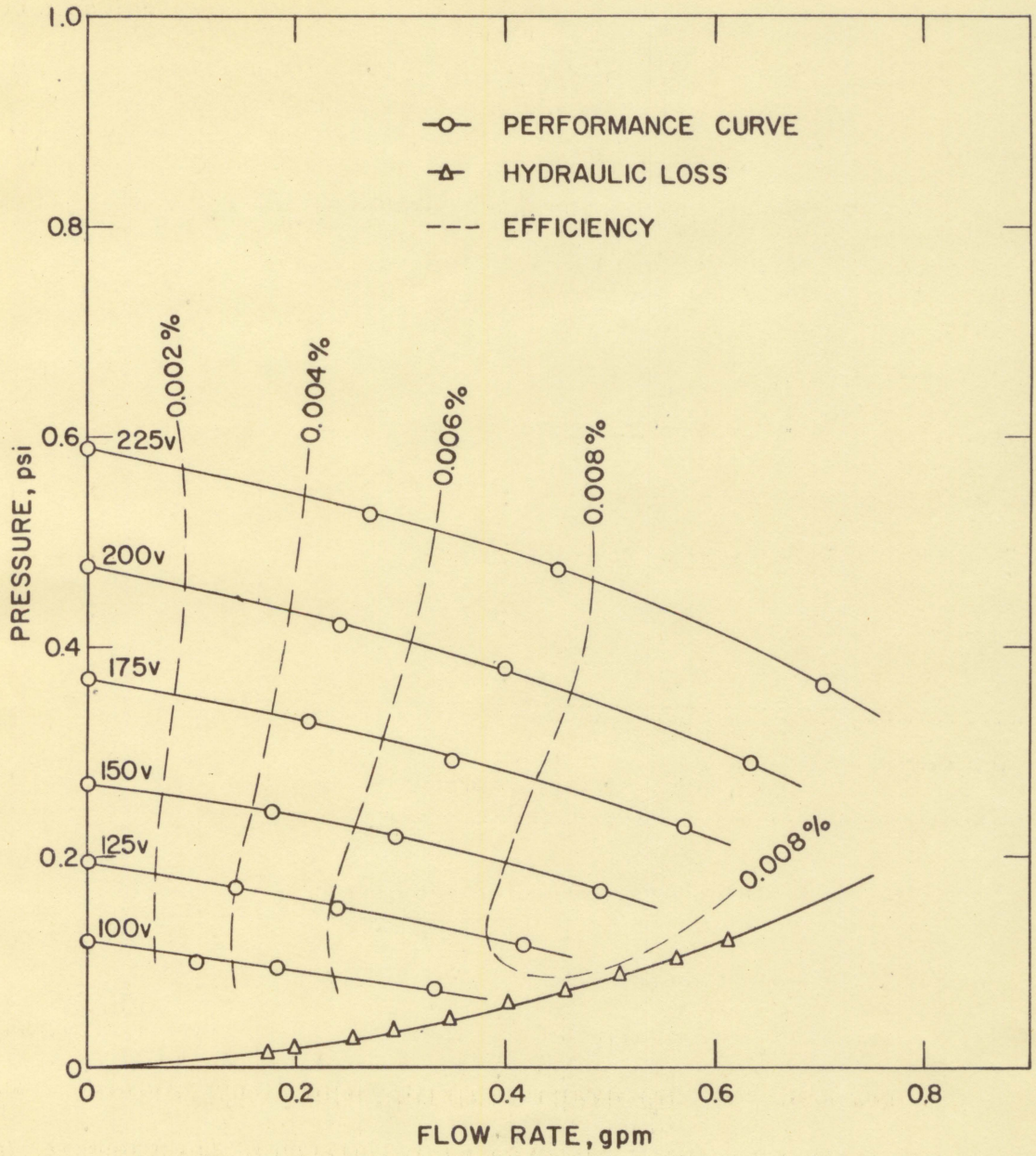

Figure 5. Induction pump performance characteristics (47 laminations, 0.250-inch duct thickness, 0.143-inch air gap)

Many of the pump sections used in large linear induction pumps are fabricated in a rectangular shape. Side bars are easily brazed to the flat edges of rectangular pump sections, as indicated in Figure 6.

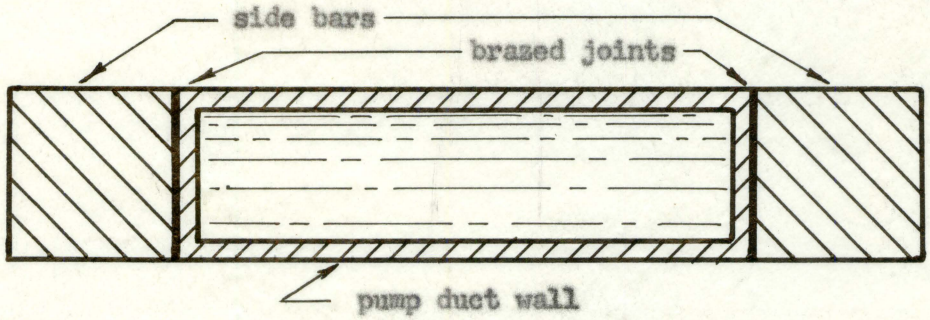

Figure 6. Cross section of a rectangular pump section with side bars

The cross-sectional view of the pump section with a 0.125-inch pump duct thickness is shown in Figure 7. The geometry of the inconel-sheathed, tantalum pump sections is not conducive to simple external side bar fabrication. It would be necessary to machine the side bars to fit the contour of the pump section, as shown in Figure 8.

Because of the high resistivity of the inconel sheath, the lack of a metallurgical bond at points of contact between the tantalum pump duct wall and inconel sheath with resulting poor electrical contact, and the separation between the tantalum and inconel at the edges of the duct, the use of side bars fabricated to the outside of the pump sections as a means of improving pump performance was questionable. It was adjudged necessary, under these conditions, to insert the side bars directly in the pump duct to assess their value accurately. The side bars were two 0.250-inch round copper rods the length of the pump maintained at the outer edges of the duct. Figure 9 shows representative copper side bars

Figure 7. Cross section of a pump section with 0.125-inch duct thickness

Figure 8. Position of external side bars

Figure 9. Copper side bars in the pump duct

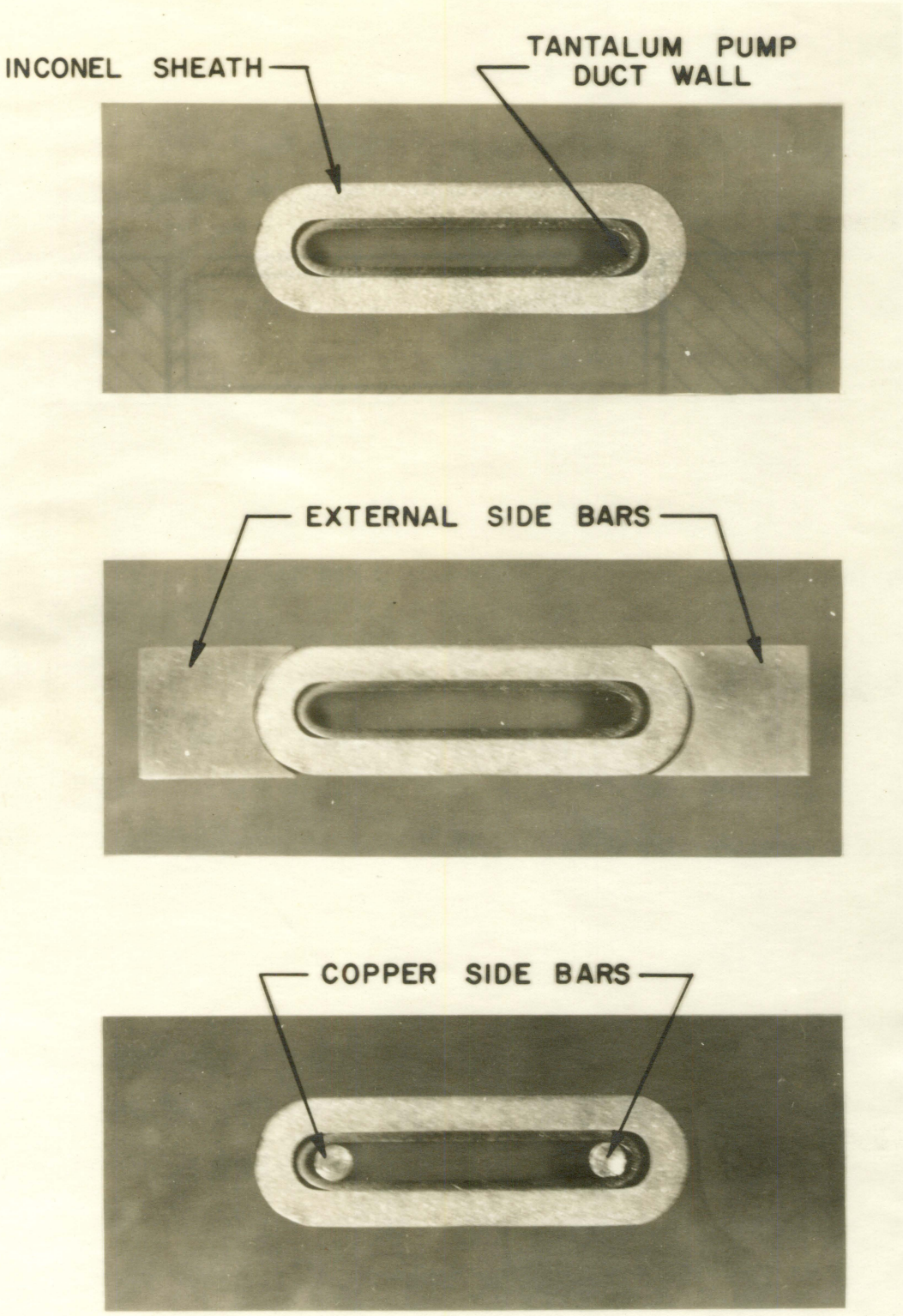
INCONEL SHEATH
TANTALUM PUMP DUCT WALL
EXTERNAL SIDE BARS
COPPER SIDE BARS

in a pump section with 0.125-inch duct thickness.

The side bars in the pump duct are in contact with only the liquid metal. The decrease in resistance to eddy current flow in the liquid metal because of the high conductivity of the copper side bars is not provided the eddy currents induced in the tantalum or inconel. Thus, the currents induced in the tantalum and inconel remain at the same magnitudes as if no side bars were present. If effective external side bars could be brazed to the pump section, the eddy currents in the tantalum and inconel would also rise. The side bars in the pump duct are advantageous as a means of increasing the eddy currents in the liquid metal without increasing the eddy currents and the I^2R losses in the tantalum pump duct wall and inconel sheath.

Copper side bars, having a resistivity of 1.85 microhm-cm at 85 F, allow a current density 52.4 times larger than that in the equivalent geometry of mercury for the same voltage drop. The decreased voltage drop in the direction parallel to the fluid flow permits a larger voltage drop across the duct, increasing the eddy currents and pressure generated. The copper side bars were chrome-plated for the first run to prevent wetting of the copper by the mercury, thus maintaining the non-wetted conditions that have existed in the pump duct.

The performance characteristics of the 47 lamination pump with chrome-plated copper side bars are shown in Figure 10. The use of these side bars approximately doubled the no-flow pressure produced without the side bars and improved operating efficiency.

Use of copper side bars produced a pronounced improvement in both

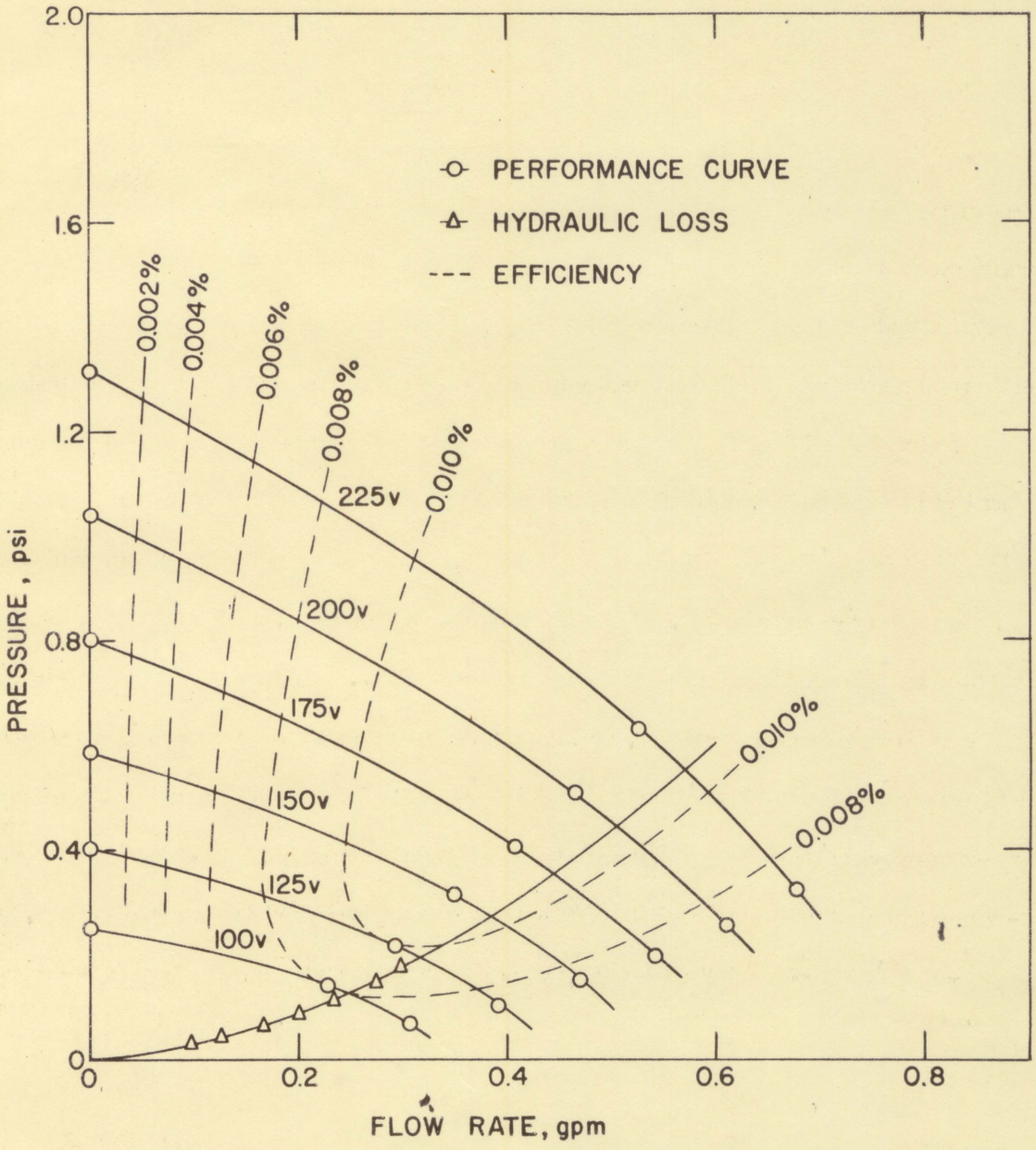

Figure 10. Induction pump performance characteristics (47 laminations, 0.250-inch duct thickness, 0.143-inch air gap, chrome-plated Cu side bars)

pressure and efficiency, as shown in Figure 11, due entirely to the wetting of the copper side bars by the mercury. The use of side bars did not alter the phase current requirement, as indicated in Table 3.

Table 3. Effect of side bars at constant voltage

side bar	voltage, volts	phase current, amperes	power, watts	no-flow pressure, psi
none	100	9.1	160	0.119
chrome-plated Cu	100	9.1	170	0.249
Cu	100	9.2	210	2.330

The increase in pressure with the use of the copper side bars is indicative of the magnitude of the eddy currents produced in the liquid metal and is inversely proportional to the total resistance of the eddy current "paths." Of special importance is the 10-fold increase in pressure due to the destruction of the interface that existed between the mercury and copper in the non-wetted condition. This indicates the resistive nature of the interface.

The wetted copper side bars are an approximation to the infinitely conducting side bars described in the development of induction pump theory. The theoretical developed pressure for this pump from equation (11), with v_s = 60 feet per second, $n\lambda$ = 12 in., ρ = 96.73 microhm cm, and B^2_{rms} = 7.220(10^5) gauss^2, is 6.04 psi. The wetted copper side bars, although providing a low resistance path for the eddy currents, are far from being the infinitely conducting side bars referred to in the

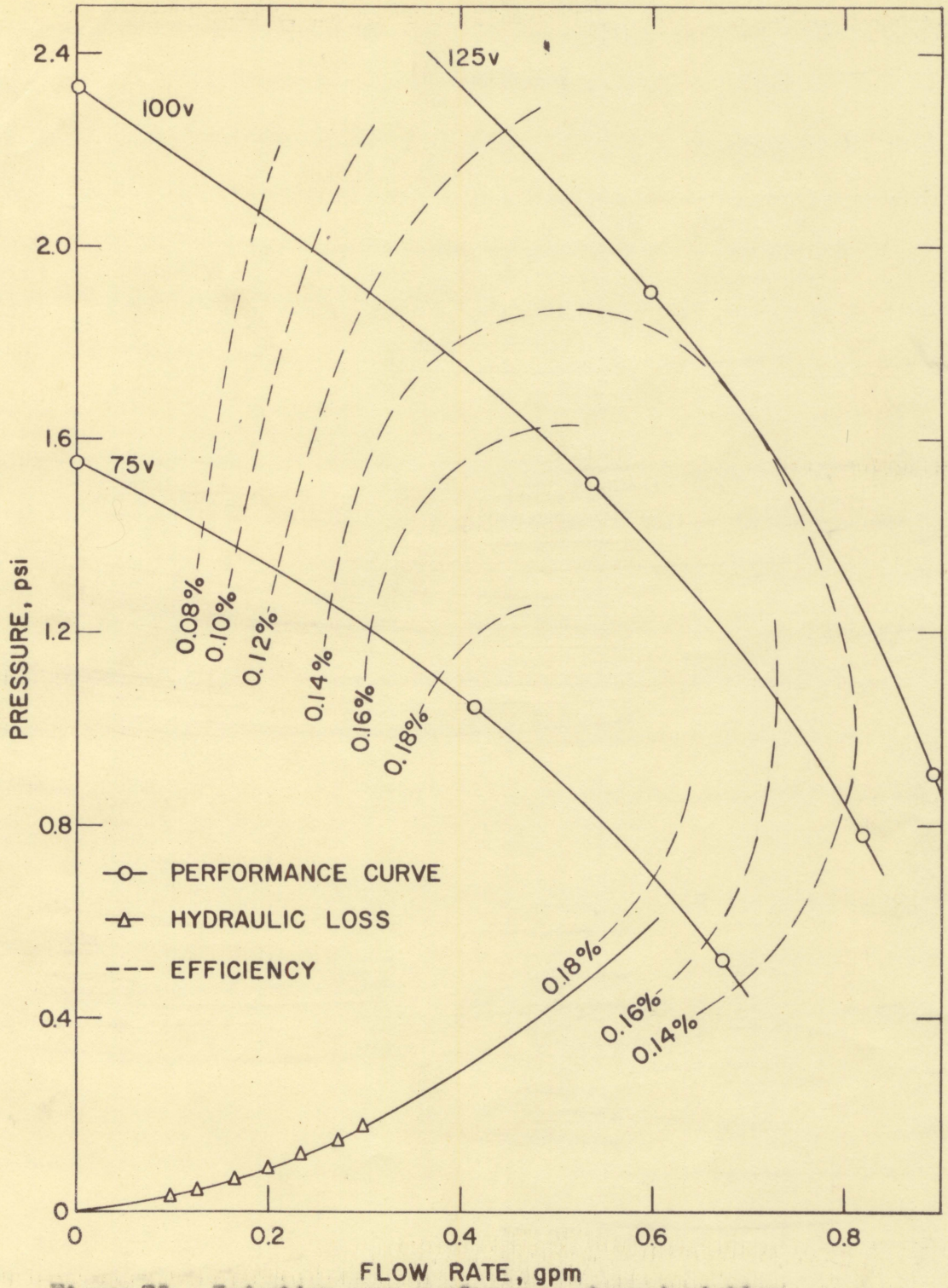

Figure 11. Induction pump performance characteristics (47 laminations, 0.250-inch duct thickness, 0.443-inch air gap, Cu side bars)

development of pumping theory. In addition, the stationary pulsating magnetic fields at the ends of the stators, the eddy currents in the liquid outside the magnetic field, and other non-ideal characteristics of this pump further remove it from ideal behavior. However, the 2.33 psi produced with the wetted copper side bars is nearly 40% of the pressure predicted from ideal induction pump theory.

D. Duct Modification

A material with the conductivity of copper that could serve as a side bar in the pump duct and be compatible with corrosive liquid metals at high temperature is nonexistent as yet. The effect of side bars can be obtained in part by the use of wider pump ducts. The increase in cross-sectional area of a pump duct with increase in pump duct width should effect a corresponding decrease in current density and resistance to current flow in the liquid metal although the length of eddy current "paths" may be increased.

Three pump sections made of electrical conduit were used to determine the effect of an increasing pump duct width on the pump performance characteristics. The 3/4-, 1-, and 1 1/4-inch (nominal) conduit, when rolled to a duct thickness of 0.250 inch, produced pump sections with duct widths of 1.164, 1.505, and 2.074 inches respectively.

To illustrate the effect of pump duct width on performance characteristics, independent of the pump used in the experiment, the variables were plotted as a function of the pump duct width/pump width ratio. The no-flow pressures produced were plotted on a relative basis with the

pressure developed at 100 volts for the 0.765 pump duct width/pump width geometry taken as unity. This was done to avoid confusion between these pressures and the pressures characteristic of the pump with the inconel-sheathed, tantalum pump sections.

Unlike previous improvements in pressure as a result of phase current increase, the increase in pressure with increasing pump duct width was accompanied by a decrease in phase current, as shown in Figure 12. The near-linear increase of pressure with increase in pump duct width verifies the effect of decreasing the eddy current density and the rate of increase is proportional to the magnitude of the eddy currents induced in the liquid metal.

The voltage in a three wire, Y connected, system with unbalanced load, as in the pump, must be distorted to allow the vectorial sum of phase currents to be zero. Power factor determined from an analyzer for such a system is meaningless. Thus, power factor for this system will be defined as

$$\text{power factor} = \frac{\text{input power}}{\sqrt{3}\,\frac{\sum \text{line voltage}}{3}\,\frac{\sum \text{phase current}}{3}} \qquad (20)$$

The power factor and average phase current indicated in Figure 12 at constant voltage are tabulated in Table 4 with other individual phase data for the three conduit pump sections. In each case, a and A refer to the coil at the inlet end of the pump, b and B refer to the center coil, and c and C refer to the coil at the outlet end of the pump.

A characteristic of the small pump duct width/pump width ratio of

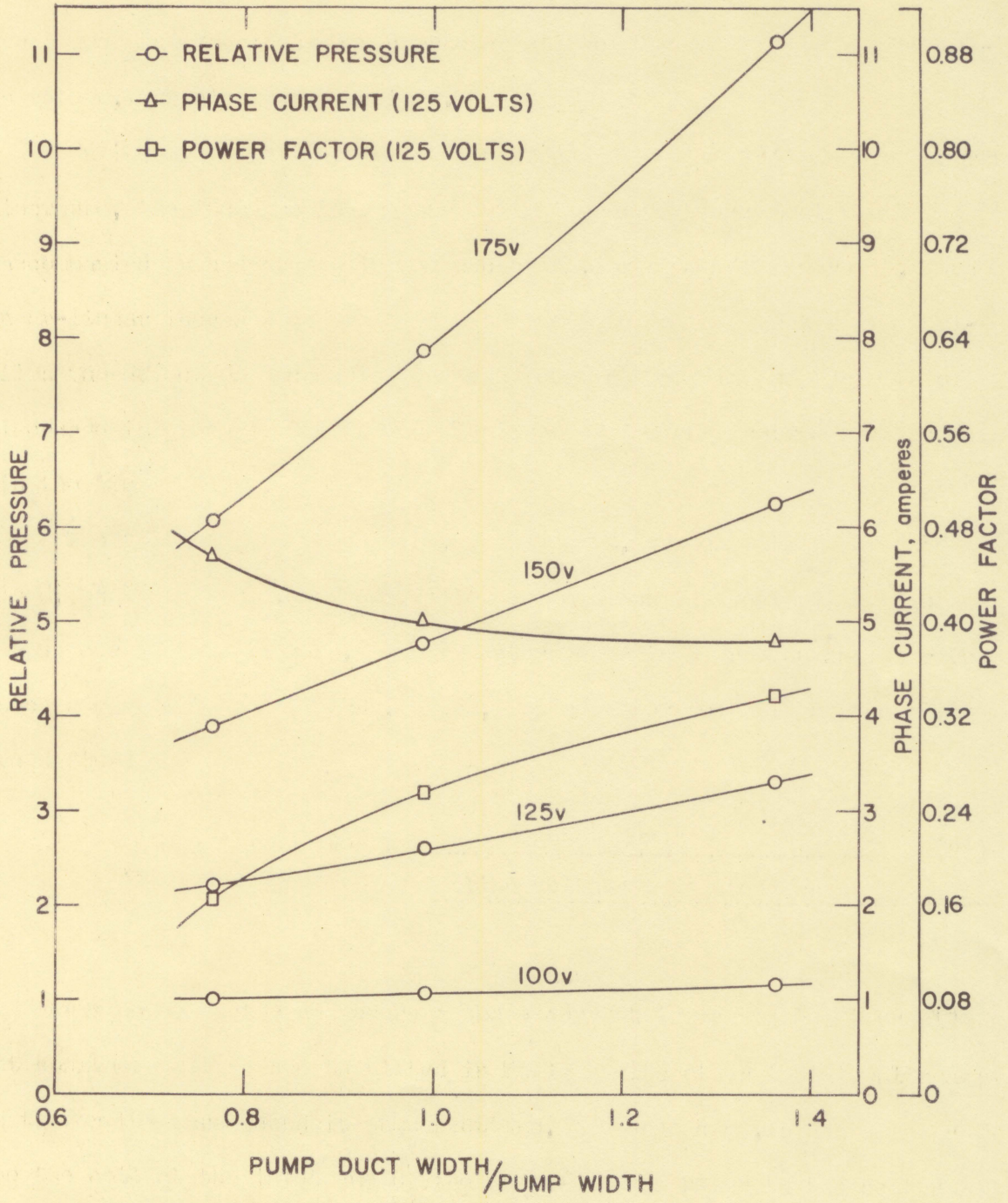

Figure 12. Pump duct width effects

Table 4. Induction pump phase parameters ar constant voltage

pump duct width/pump width	line voltage volts			phase voltage volts			phase current amperes		
	Eab	Ebc	Eca	Ean	Ebn	Ecn	A	B	C
0.765	131	130	129.6	82.0	66.0	82.4	6.1	4.9	6.0
0.988	132	130.4	130.2	82.0	66.5	82.1	5.44	4.3	5.2
1.361	131.8	130.2	129.2	81.0	64.8	80.8	5.16	4.18	4.96

pump duct width/pump width	phase power watts			phase power factor			average power factor	relative no-flow pressure
	A	B	C	A	B	C		
0.765	183	59	-21	0.366	0.183	-0.043	0.165	2.19
0.988	191	77	18	0.428	0.274	0.042	0.254	2.58
1.361	210	100	53	0.502	0.369	0.132	0.337	3.3

0.765 is the negative power input to coil C. This means the current in coil C is out of phase more than 90° with the voltage and implies that the liquid metal is returning power to the coil as it leaves the pump.

Because of the high slip and the three phase windings on a common magnetic core, the windings of the pump are capable of acting as the primary of a three phase transformer. A negative power condition can be produced in one phase of a three phase transformer if the transformer is supplying an unbalanced inductive load. The unbalanced load existing in this pump at the relatively low pump duct width/pump width ratio of 0.765 may have been sufficient to produce the negative power condition.

E. Magnetic Field Strength

The magnetic field strength of the pump was calculated from the induced voltage in a small search coil. The values of field strength, as shown in Figure 13, for a representative pump geometry, indicate a linear increase of field strength with voltage. At these values of field strength no tooth saturation is evident and the low field strength at the ends of the stator minimizes the losses incurred because of stator discontinuity.

The large drop in field strength across the slots in the stator is a result of the large air gap and decreases the mean value of field strength over the entire length of the pump to approximately 0.6 the magnitude of highest flux produced.

The magnetic field of an annular induction pump produced by a Y connected, one slot per pole per phase, winding has been shown to have

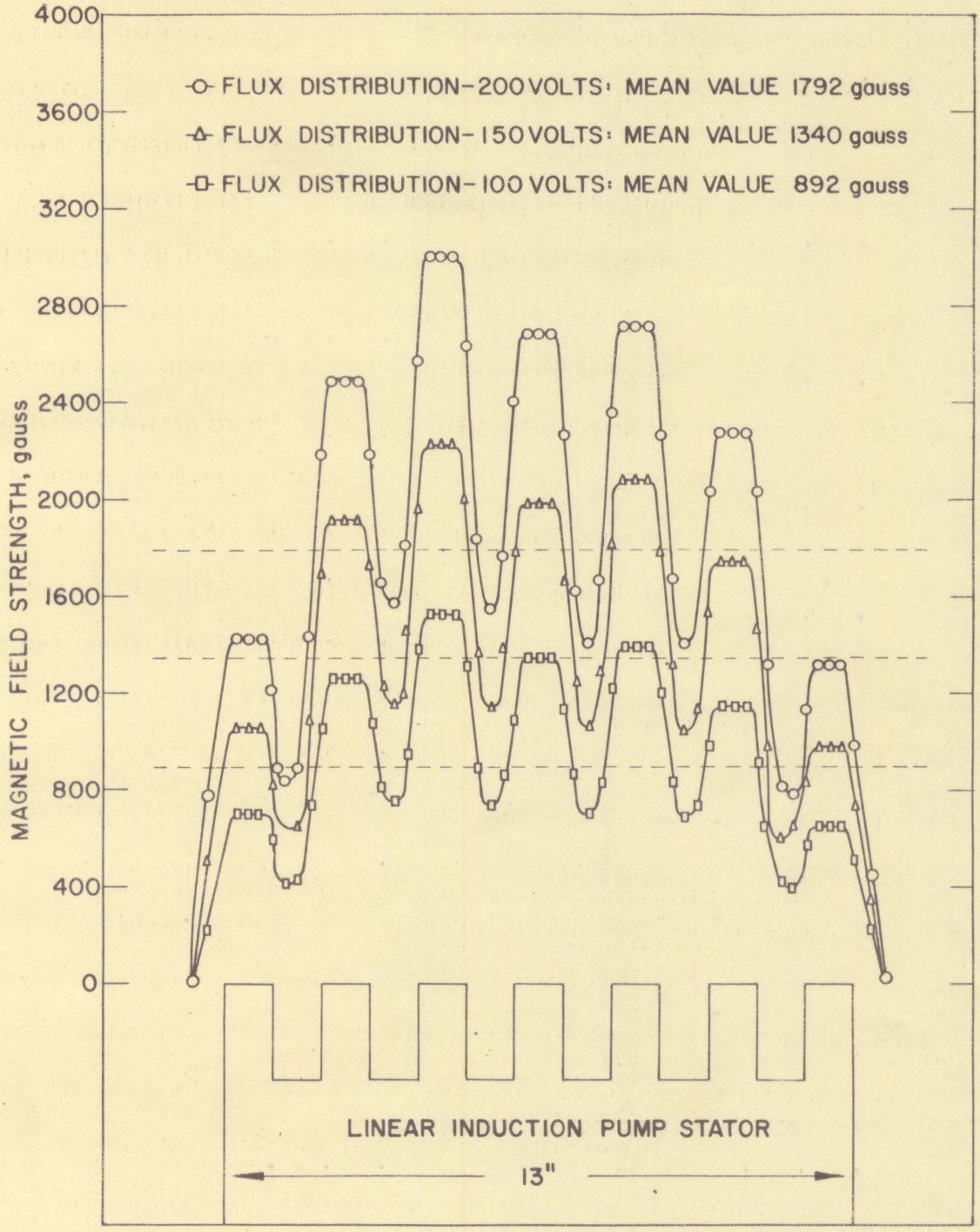

Figure 13. Linear induction pump magnetic field strength (76 laminations, 0.443-inch air gap)

strong fifth and seventh harmonics (17). The fifth harmonic, traveling in a direction opposite to that of the fundamental, and the seventh harmonic, traveling in the same direction as the fundamental but at a slower speed, both produced a braking action in the liquid.

There is no reason to believe that harmonics do not exist in the magnetic field produced by the linear induction pump. However, the waveform of the search coil output at each measured point along the stator, observed with an oscilloscope, was sinusoidal in nature and none but the fundamental wave was observed. Any existing harmonics were undetected and thus their effect is neglected in this discussion.

Figure 13 does not indicate the instantaneous field values, but indicates the maximum rms value of the field reached at any time resulting from the combined effect of all three phases. The instantaneous flux distribution in the air gap of the pump, at 100 volts, is plotted in Figure 14. These curves were produced by synthesis of the individual phase flux distributions. The individual phase flux distributions were obtained by operating each coil separately at the same current, also the same ampere turns, that was drawn by that coil when operating from the three phase power supply. The currents in the three coils were assumed to be displaced the normal 120 electrical degrees, as shown at the top of Figure 14. The magnitude of the current, direction of current flow, direction of coil insertion in the stator, and the resulting direction of flux at each point in the stator for each coil were other considerations necessary in the instantaneous flux distribution calculations. The calculations were made for the four instants of time T_1, T_2, T_3, and T_4, with

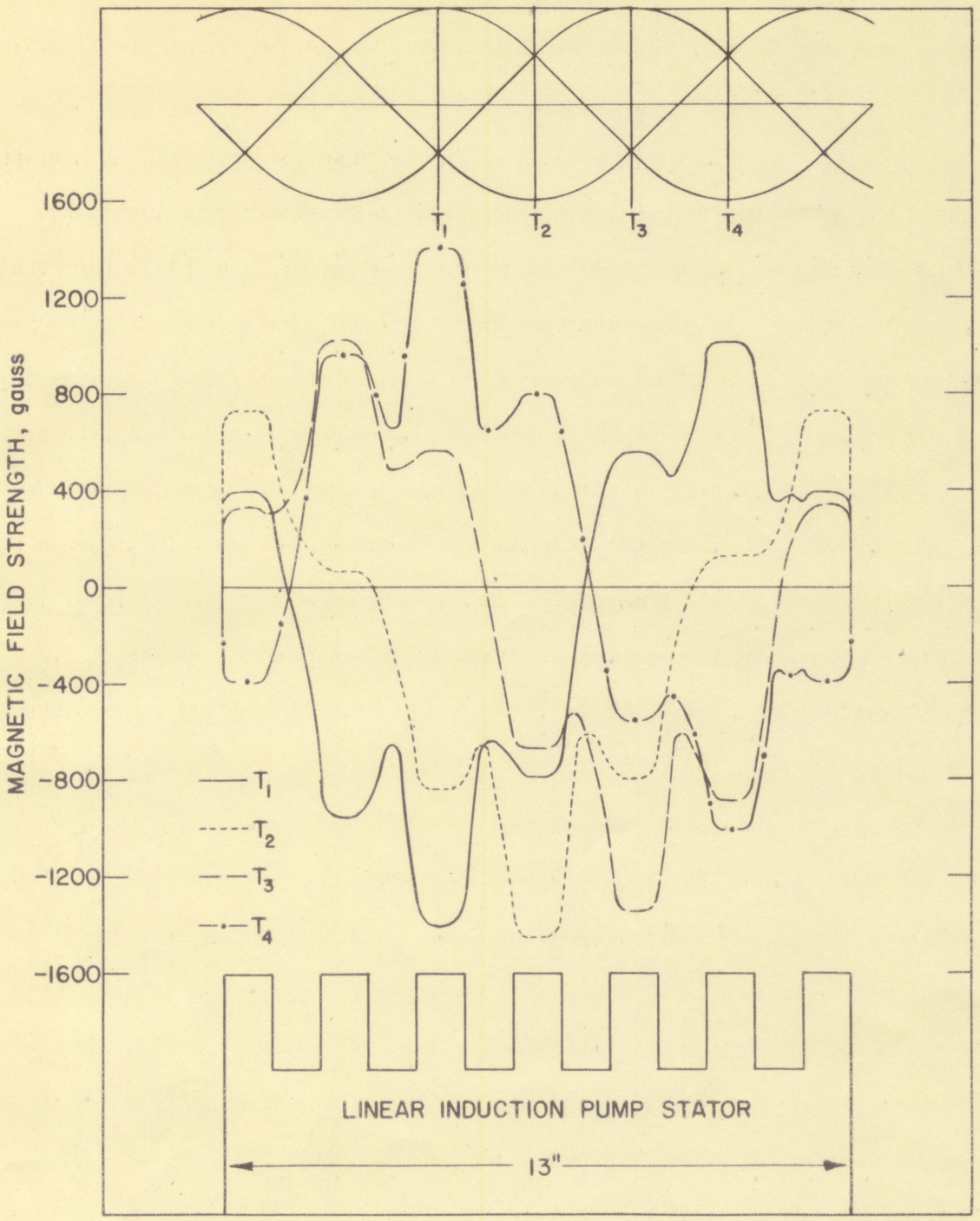

Figure 14. Instantaneous flux distribution at 100 volts (76 laminations, 0.043-inch air gap)

60 electrical degree spacing between adjacent time instants.

Figure 14 furnishes visual evidence of the moving magnetic field. The distance moved by the field in 60 electrical degrees is the distance between adjacent pole faces, or two inches. In one cycle (360 electrical degrees) the field moves one foot and with 60 cycles per second power the velocity is 60 feet per second. The area bounded by the instantaneous flux distribution curves remains nearly constant, indicating that the effective flux does not vary with time. Thus, the three phase windings produce a constant effective magnetic field that travels at a uniform velocity.

The waveform of the ideal flux distribution is sinusoidal in nature. Control of the waveform is obtained in the design of the windings and the layout of the coils making up the stator windings. The flux distribution in the air gap of this pump is not sinusoidal, as indicated in Figure 14. This is a result of the single coil per phase winding, but the waveform can be improved by increasing the number of slots per pole to provide a distributed winding over the stator length.

Figure 13 is actually the envelope of all instantaneous flux distribution curves. The average value of B^2_{rms} from Figure 13 was obtained by squaring each ordinate of the curve and measuring the total area under the resulting curve with a planimeter. Division of the total area by the length of the stator provided the average value of the field strength over the length of the pump. The same procedure was used to determine the effective value of B^2_{rms} from Figure 14. At 100 volts, the average value of B^2_{rms} from Figure 13 was $1.041(10^6)$ gauss^2 and the effective

value of B^2_{rms} from Figure 14 was 0.518(10^6) $gauss^2$. The effective value of B^2_{rms} is half that determined from the maximum flux density distribution. This relationship permits the calculation of the effective value of B^2_{rms} from the measured three phase flux distribution and is much simpler than individually measuring each phase flux distribution in order to arrive at the same value.

The nonmagnetic characteristic of the pump section materials will not diminish these values, but the magnetic fields produced in the liquid metal by the large eddy currents may be large enough to decrease the effective value of the field in the liquid metal.

The effective magnetic field strength produced in the 0.443-inch air gap, irrespective of the number of laminations in the stators, is approximately 78 gauss/amp. This value is increased to 103 gauss/amp with a decrease in air gap to 0.310 inch. The result of the constant magnetic field per unit current excitation was indicated in Table 2 as a nearly constant no-flow pressure developed, irrespective of the number of stator laminations, for a constant phase current.

The I^2R losses in the windings of some linear induction pumps have been halved by placing windings in both the upper and lower stators. The same ampere turns excitation can then be obtained with half the current supplied to each winding group. This was attempted with the linear induction pump by removing the top stator and replacing it with the bottom stator from another pump. The coils directly opposite each other across the pump section were fed from the same phase so not to disturb the traveling field by having the coils out of phase.

Transformer action by one group of coils was detrimental to the operation of the other coil group. The induced effects caused by one winding group had to be overcome by the second group before any contribution to the magnetic field strength by the second coil group could be made. The maximum magnetic field strength produced by the operation of a single winding group was comparable to that obtained in the regular linear induction pump at the same voltage. Operation of both winding groups produced a flux that was only 20% higher than that produced by one winding group. However, the depression of the flux was much more severe across the slots, now on both sides of the pump section, than for the regular pump geometry. Thus, the effective value of the magnetic field was about the same as for the regular pump geometry.

At 150 volts and above the pump vibration increased markedly. This vibration indicated that the coils might not have been phased properly for correct operation. Corrective measures were not taken because the large depression of the flux across the slots nullified the increased flux at the pole faces.

VII. SUMMARY AND CONCLUSIONS

The linear induction pump (76 laminations, 0.125-inch duct thickness, 0.319-inch air gap) can produce a maximum no-flow pressure of 0.734 psi and can pump 0.450 gpm against a 0.2 psi head. With an air gap of 0.443 inch and a pump section having a 0.250-inch duct thickness, the maximum no-flow pressure decreases to 0.551 psi, but the improved hydraulic efficiency of the larger duct permits circulation of 0.9 gpm against a 0.2 psi head. The improvement in magnetic field strength from 78 gauss/amp at 0.443 inch air gap to 103 gauss/amp at 0.310 inch air gap indicates the need for minimizing the pump air gap while maintaining a duct thickness consistent with good hydraulic efficiency.

With the same pump and pump section geometry, the use of chrome-plated copper side bars doubled the pressure developed by the pump without side bars. Copper side bars wetted by the mercury produced a 20-fold improvement in developed pressure and increased the pumping efficiency from 0.010% to 0.18%. The pump performance with the wetted copper side bars was nearly 40% of that predicted for an ideal induction pump. This indicates the utmost importance of fluid wetting for good pump performance and efficiency.

The relatively good conductivity of tantalum, a major factor in the poor pump efficiency, can be used to improve the performance characteristics of the pump. Although they are less effective than copper as side bars, tantalum side bars will improve the performance characteristics of the pump when operating at high temperatures with high resistivity liquid metals. In order to retain the performance improvements obtained with

side bars, sufficient flow area must be provided to prevent hydraulic losses from nullifying the side bar effect.

As shown in Figure 7, the tantalum does not touch the inconel at the edges of the pump duct, thus the electrical continuity and any possible side bar effects of the inconel sheath are lost. The inconel should be reduced in thickness to the minimum consistent with strength and other sheathing requirements and the tantalum tubing should fit tightly against the inconel. This may be accomplished by swaging the reduced inconel pipe on the tantalum tubing prior to rolling the pump section.

Increase of the pump duct width is beneficial to improved pump performance. The increase in pump duct width is accompanied by an increase in power factor and a decrease in phase current. In addition, the increased flow area decreases the hydraulic losses and decreases the eddy current density in the direction of fluid flow. The decrease in eddy current density improves pressure generation by the pump, particularly at high voltage, and the added fluid in the pump duct is, in effect, a liquid side bar.

The magnetic field strength of the pump does not produce an apparent saturation of the stator laminations. However, because of the large slot widths in the stator, the mean value of the field strength is reduced to just 0.6 of the maximum values reached.

The phenomenon of fluid wetting of the pump duct wall and the use of side bars provide powerful tools for improving the linear induction pump performance characteristics. Full advantage of the improved performance can be obtained if the hydraulic losses are minimized by using

a pump section with large duct width, which also improves the power factor and decreases the phase current requirements of the pump.

VIII. SUGGESTIONS FOR FURTHER INVESTIGATION

If induction pump design could conceivably be considered in just two phases, the first phase would encompass winding and stator design for maximum magnetic field strength and the second would be concerned with the utmost utilization of the magnetic field produced.

The most desirable waveform of the traveling magnetic field is a sinusoid. The single slot per pole per phase winding of the linear induction pump studied produces a stepped magnetic field, but this can be improved by using a distributed winding with an increase in the number of slots per pole. A reduction of the losses incurred as a result of the pulsating magnetic field at the stator ends and an improvement in the production of a nearly pure traveling wave can be realized by one of several methods of winding the end poles of the stator to gradually increase the magnetic field. In practice the double layer winding lends itself admirably to field grading, which is the term given these winding methods. The use of a single winding on the end poles of the stator allows the magnetic field strength to be increased gradually at the ends of the stator and reduces the magnitude of the eddy currents flowing in the liquid outside of the magnetic field.

Because of the lack of parallel in induction motor theory of the discontinuous stator and the resulting pulsating magnetic field, and the relative newness of electromagnetic pumping, the discontinuity phenomenon and magnitudes of the losses incurred as a result are not adequately understood. Research in this area should produce a better ability to predict performance characteristics of electromagnetic pumps than currently

exists.

The investigation of side bar effect and duct modification on the performance characteristics of the linear induction pump as summarised in this thesis by no means exhausts the possibility of further research in this area. The study of eddy current distortion of the magnetic field, effect of change in the number of poles, and effect of pole pitch on the pump performance characteristics are but a few of the many variables that need to be studied in order to further the understanding and development of electromagnetic pumping.

IX. LITERATURE CITED

1. AEC puts together a long-range power reactor program. Nucleonics 18, no. 4: 71-82. April 1960.

2. Power cost normalization studies. United States Atomic Energy Commission Report SL-1674 [Sargent and Lundy, Chicago]. September 1, 1959.

3. Northrup, Edwin F. Some newly observed manifestations of forces in the interior of an electric conductor. Physical Review 24: 474-497. 1907.

4. Feld, B. and Szilard, L. A magnetic pump for liquid bismuth. United States Atomic Energy Commission Report CE-279 [Chicago. Univ. Metallurgical Lab.]. July 14, 1942.

5. Tama, Mario. Electromagnetic pumping of molten metals. The Iron Age 160, no. 23: 68-70. December 4, 1947.

6. Watt, D. A. The design of electromagnetic pumps for liquid metals. United Kingdom Atomic Energy Authority Report AERE R/R 2572 [Gt. Brit. Atomic Energy Research Establishment, Harwell, Berks, England]. 1958.

7. Blake, L. R. Conduction and induction pumps for liquid metals. The Proceedings of the Institution of Electrical Engineers, Part A, 104: 49-67. 1957.

8. _____. Electro-magnetic pumps for liquid metals. Journal of Nuclear Energy, Part B, 1: 65-76. 1959.

9. Jaross, R. A. and Barnes, A. H. Design and operation of a 10,000 gpm d.c. electromagnetic sodium pump and 250,000 ampere homopolar generator. 2d United Nations International Conference on the Peaceful Uses of Atomic Energy. Paper A/Conf. 15/P/2157. June 1958.

10. Seim, Orville S. and Jaross, Robert A. Characteristics and performance of 5000 gpm ac linear induction and mechanical centrifugal sodium pumps. 2d United Nations International Conference on the Peaceful Uses of Atomic Energy. Paper A/Conf. 15/P/2158. June 1958.

11. [Findlay, Gordon R.] General description of the electrodynamic pump. (Mimeo.) Westford, Mass., Liquid Metals, Inc. [1957.]

12. Fisher, Ray W. and Fullhart, Charles B. Feasibility studies on molten metal reactor components. 2d United Nations International Conference on the Peaceful Uses of Atomic Energy. Paper A/Conf. 15/P/1032. June 1958.

13. _____ and Winders, G. R. High-temperature loop for circulating liquid metals. Chemical Engineering Progress Symposium Series 53, no. 20: 1-6. New York, N.Y., American Institute of Chemical Engineers. 1957.

14. American Society of Mechanical Engineers. Research Committee on Fluid Meters. Fluid meters. 5th ed. New York, N.Y., Author. 1959.

15. Raseman, C. J. and Weisman, J. Liquid metal fuel reactor (LMFR) processing loops. Part 1. United States Atomic Energy Commission Report BNL 322 [Brookhaven National Lab., Upton, N.Y.]. June 1954.

16. Watt, D. A. Electromagnetic pumping of liquid metals. United Kingdom Atomic Energy Authority Report AERE ED/R 1824 [Gt. Brit. Atomic Energy Research Establishment, Harwell, Berks, England]. 1956.

17. Asti, Jacob F. Development of electromagnetic pumps for liquid metals. United States Atomic Energy Commission Report NP 4892 [Technical Information Service Extension, AEC]. June 30, 1952.

X. ACKNOWLEDGMENTS

Appreciation and thanks are extended to Dr. Glenn Murphy and Mr. Ray Fisher for their guidance and encouragement in making this study. Appreciation is expressed to the Electrical Engineering Department and to its members who provided assistance and counsel.

Also recognition should be accorded certain members of the Nuclear Engineering Group II of the Ames Laboratory for their encouragement and assistance.

XI. APPENDIX

The pressure drop of mercury through each pump duct was calculated from pressure drop measurements made with water. Equivalence of the frictional coefficient in a pump duct for water and mercury was established by equivalence of the Reynolds number

$$\left[\frac{\rho v d}{\mu}\right]_{H_2O} = \left[\frac{\rho v d}{\mu}\right]_{Hg} \tag{21}$$

where

ρ = density

v = velocity

d = equivalent pump duct diameter

μ = viscosity

Because pressure loss calculations for mercury in a pump duct were made from pressure drop measurements in the same duct, the equivalent diameter remained the same for either fluid. Thus,

$$v_{Hg} = v_{H_2O}\left[\frac{\rho_{H_2O}}{\rho_{Hg}}\right]\left[\frac{\mu_{Hg}}{\mu_{H_2O}}\right] \tag{22}$$

Each fluid can be considered as incompressible at the low pressures involved and from the continuity equation for incompressible fluids the flow rates are directly related to the fluid velocities.

$$Q_{Hg} = Q_{H_2O}\left[\frac{\rho_{H_2O}}{\rho_{Hg}}\right]\left[\frac{\mu_{Hg}}{\mu_{H_2O}}\right] \tag{23}$$

From the Darcy formula for each fluid

$$H = f \frac{l}{d} \frac{v^2}{2g} \tag{24}$$

where

H = head loss

f = frictional coefficient

l = length of tubing

d = equivalent pump duct diameter

v = velocity

g = acceleration of gravity

the pressure drop is given by

$$\Delta p = H w \tag{25}$$

with

$$w = \rho g \tag{26}$$

where

w = specific weight

Thus,

$$\Delta p = f \frac{l}{d} \frac{v^2}{2} \rho \tag{27}$$

Equality of the frictional coefficient at equal Reynolds number provides a means of relating the pressure drops of the two fluids.

$$\left[\Delta p\right]_{Hg} = \left[\Delta p\right]_{H_2O} \left[\frac{v_{Hg}}{v_{H_2O}}\right]^2 \left[\frac{\rho_{Hg}}{\rho_{H_2O}}\right] \tag{28}$$

Combining equation (22) and (27) yields

$$\left[\Delta p\right]_{Hg} = \left[\Delta p\right]_{H_2O} \left[\frac{\rho_{H_2O}}{\rho_{Hg}}\right] \left[\frac{\mu_{Hg}}{\mu_{H_2O}}\right]^2 \qquad (29)$$

Equation (29) was the expression used to calculate the pressure drops in the pump ducts for mercury from the pressure drop measurements made with water.